Investigation of the structure of water at hydrophobic and hydrophilic interfaces by angle-resolved TIR Raman spectroscopy

Journal:	*Physical Chemistry Chemical Physics*
Manuscript ID:	CP-ART-06-2015-003581.R1
Article Type:	Paper
Date Submitted by the Author:	23-Aug-2015
Complete List of Authors:	Ota, Chikashi; HORIBA, Ltd, Advanced R&D Center

Investigation of the structure of water at hydrophobic and hydrophilic interfaces by angle-resolved TIR Raman spectroscopy

Chikashi Ota[a]

[a] Advanced R&D Center, Horiba, Ltd., Horiba, Ltd., Miyanohigashi, Kisshoin, Minami-ku, Kyoto 601-8510, Japan

Corresponding Author:

Chikashi Ota

Advanced R&D Center,

Horiba, Ltd,

2 Miyanohigashi, Kisshoin, Minami-ku, Kyoto 601-8510, Japan

Tel: 81-75-325-5037

Fax: 81-75-315-3806

E-Mail: chikashi.ota@horiba.com

Abstract

To analyse the surface- or interface-specific molecular structure of a condensed molecular system, it is important to measure the spectra of molecules near the surface. Total internal reflection (TIR) Raman spectroscopy is a sensitive technique for surface or interfacial analysis because it retrieves spectra in the region within ca. 100 nm of a surface. However, since the width of the interface itself is often molecular in scale (one to a few nm), conventional TIR Raman spectroscopy intrinsically lacks surface sensitivity.

To overcome this problem, the combination of multiple-angle TIR Raman spectra and principal component analysis (PCA) is expected to enable effective differentiation between the spectra of minute chemical species at the interface and those of dominant species. In the present study, angle-resolved TIR Raman spectroscopy with PCA was applied to SiO_2/water and SAM/water interfaces to detect minute species located within a few nm of each interface. This method will likely lead to progress in various surface and interfacial analyses, not only those related to the structure of water, but also those used to determine the interactions among absorbed species.

Keywords: TIR-Raman spectroscopy, principal components analysis, Interface analysis

Introduction

Various analytical methods have been developed to investigate surface- or interface-specific molecular structures in condensed molecular systems. One approach is topographical observation by using techniques such as scanning electron microscopy (SEM) and scanning probe microscopy (SPM). However, it is sometimes difficult to observe the molecular interaction and conformation of each functional group using these techniques. In contrast, spectroscopic analyses such as infrared spectroscopy, Raman spectroscopy and nonlinear spectroscopy are powerful methods that can reveal the molecular orientation, conformation and interaction of each functional group.

Some spectroscopic methods have been reported for the analysis of surfaces/interfaces, for example spectroscopic selection rules such as sum frequency generation (SFG) spectroscopy.[1,2] SFG, which is a second-order nonlinear technique that yields no signals from centrosymmetric or isotropic media, can be used to study interfacial structures at the molecular level. However, SFG has non-trivial disadvantages such as high instrument cost, complex system adjustment and difficult signal interpretation.

Another surface/interface analysis method is confocal Raman microscopy.[3,4] Although this method is practical and powerful, its spatial resolution is limited by the diffraction limit, and the smallest theoretical spatial resolution is almost half of the wavelength determined by Abbe's equation. In reality, the spatial resolution of confocal Raman microscopy is about 1 μm, and the depth resolution is about 2 μm.[3,4]

Another technique is total reflection spectroscopy using evanescent fields such as attenuated total reflection infrared (ATR-IR)[5,6] spectroscopy and TIR Raman spectroscopy.[7-12] The penetration depth (d_p) depends on the excitation wavelength. TIR

Raman spectroscopy is more surface-sensitive and involves shorter penetration depths (ca. 100 nm), since it uses visible light as the excitation source. However, TIR Raman spectroscopy is not widely used, and its application is limited to a small number of researchers; in contrast, ATR-IR spectroscopy is a well-known method, and commercial ATR-IR spectroscopy instruments are already widespread.

The reason why ATR-IR spectroscopy is significantly more popular than TIR Raman spectroscopy is because the signal intensity of IR spectroscopy is much larger than that of Raman spectroscopy. This intensity difference exists because infrared absorption cross sections are 10 orders of magnitude larger than Raman cross sections.[12] Although the signal intensity of TIR Raman spectroscopy is weaker than that of ATR-IR spectroscopy, TIR Raman spectroscopy has two advantages in addition to a shorter d_p. One advantage is that in ATR-IR spectroscopy, the refractive index is not the same at each wavelength; therefore, the penetration depth varies across the observed spectral range. In contrast, in TIR Raman spectroscopy, the penetration depth is determined only by the excitation wavelength; thus, the penetration depth is constant across the observed spectral range. Another advantage is that the strong bands in ATR-IR spectroscopy are distorted by the rapid variations in the refractive index of a sample;[13,14] this distortion is not present in TIR Raman spectroscopy results. For these reasons, the interpretation of depth profiling analysis is simpler by TIR Raman spectroscopy than by ATR-IR spectroscopy.

Although the penetration depth of TIR Raman spectroscopy is less than 100 nm, the signal irradiated by the evanescent wave still intrinsically originates from bulk species since the width of the interface itself is often on the molecular scale (one to a few nm).[15] Therefore, TIR Raman spectroscopy lacks the intrinsic surface sensitivity of

non-linear optical methods such as SFG. The combination of multiple-angle TIR Raman spectroscopy with principal component analysis (PCA), a chemometric method, is expected to overcome this problem and enable effective differentiation between the spectra of minute chemical species within a few nm of the interface and those of dominant species.[16,17] In the present study, angle-resolved TIR Raman spectroscopy with PCA was applied to SiO_2/water and SAM/water interfaces to detect the minute species within a few nm of each interface.

Theory

If the incident medium has a refractive index larger than that of the second medium ($n_1 > n_2$), and the incidence angle θ is sufficiently large, the incident light is totally reflected at the interface, and the critical angle is given by

$$\theta_c = \sin^{-1}\frac{n_2}{n_1}. \quad (1)$$

At the interface, the light penetrates into the sample as an exponentially decaying electric field, which is called an evanescent field. The amplitude of the evanescent field (E) decreases exponentially with distance (z) according to

$$E = E_0 \exp(-k\beta z), \quad (2)$$

where E_0 is the electric field of the incident light at the interface, k is the wavevector of the incident light,

$$k = 2\pi n_2 / \lambda_0, \quad (3)$$

and β is a coefficient defined as

$$\beta = \sqrt{\left(\frac{n_1}{n_2}\right)^2 \sin^2\theta - 1}. \quad (4)$$

The penetration depth (d_p) is given by

$$d_p = \frac{\lambda}{2\pi}\left(\frac{1}{\sqrt{n_1^2 \sin^2\theta - n_2^2}}\right). \quad (5)$$

The intensity of Raman scattering is proportional to the square of the electric field; therefore, it decays twice as fast as the electric field.[10] Thus, the effective penetration depth of Raman scattering is given by

$$d_{eff} = d_p / 2. \quad (6)$$

Experimental Section

Raman Spectroscopy

The Raman spectroscopic bench was a HORIBA Jobin Yvon (Paris, France) XploRA Raman microscope with Labspec 5 software. The focal length was 200 mm,

and the optical configuration was the back-scattering geometry. An Andor (Belfast, Northern Ireland) iDus 420 thermoelectrically cooled charge-coupled device (CCD) camera was used as the detector. The entrance slit of the spectrometer was set to 100 μm. The dispersive element had a grating of 1800 lines·mm^{-1}, which provided a wavenumber resolution of ca. 2 cm^{-1}. A Coherent, Inc. (Santa Clara, CA, USA) Compass 315M solid-state CW laser (532 nm) was used as an excitation light source. The laser power was 15 mW at the sample surface, and the laser light was S-polarised using a Thorlab GLA5-A Glan-Laser. The excitation intensity was monitored using an Advantest (Tokyo, Japan) TQ8210 optical power meter. The Raman shift was calibrated using the atomic emission lines of a neon lamp.

A customized TIR unit was used to change the angle of incidence of the excitation laser. This TIR Raman unit was set on a Marzhauser Wetzlar Gmbh & Co. KG (Wetzlar, Deutschland) SCAN 100 × 100 X-Y stage. From the top side of the prism, the Raman scattering was collected through an Olympus (Tokyo, Japan) MPLN5X objective lens with a numerical aperture (NA) of 0.1. In the present system, the objective lens was used only to collect the Raman scattering, although microscope optics were employed. The hemisphere prism was an SF59 prism from Pier Optics (Gunma, Japan) with an outer diameter of 20 mm. The angles of incidence were changed within the range of 46° to 72° in 5° increments. The exposure time of the sample to the excitation light was 20 s, and 20 accumulations were performed for each measurement.

Sample Preparation

Before measuring the prism(SiO_2)/water interface, the hemisphere prism surface was cleaned with ozone using a UV/ozone dry surface processing unit (PL 12-200 Photo

Surface Processor; Sen Lights Corporation, Osaka, Japan). The total duration of UV irradiation was 10 min. The generated ozone not only reacted with surface contaminants to eliminate them, but also reacted with the surface of the prism to yield Si-OH bonds.

The surface of the prism was reacted with octadecyl trimethoxy silane (ODS) to form a self-assembled monolayer (SAM). A solution of ODS in a methlyethylbenzene-containing organic solvent (SAMLAY-A) was purchased from Nippon Soda Co., Ltd. (Tokyo, Japan).

For the prism(SiO_2)/water and prism/SAM/water interface measurements, water was obtained from a Millipore (Bedford, MA) Milli-Q laboratory water purifier. The sample holder was a custom-made anodised aluminium-coated metal plate containing a sample well with an internal diameter of 20 mm. In order to assemble the sample holder, the sample well was filled with water and covered by the prism, ensuring that no air bubbles remained at the interface. The assembled sample holder was then mounted on the sample stage.

Spectroscopic Analysis

The number of chemical species in the protein solution was estimated by PCA. PCA is a powerful chemometric method that can resolve the spectra of minute chemical species from those of dominant species.[16,17] The contribution ratio (normalised concentration, C_R) of each factor is given by,

$$C_R(j) = \frac{C_j}{\sum_{j=1}^{h} C_j}, \qquad (7)$$

where C_j is the concentration of each factor.

The accuracy of the model prediction was evaluated by rank analysis using reduced-eigenvalue (REV) plots. An REV intrinsically has the same statistical meaning as the normal eigenvalue; however, REVs are better for the evaluation of minute eigenvalues because they take the degrees of freedom into account.[16] The REV plots were obtained according to the following expression:

$$REV_j = \frac{\lambda_j}{(N-j+1)(M-j+1)}. \quad (8)$$

Here, j is the factor level, and the parameters N and M express the dimensions of the spectral matrix ($N \times M$). Notably, the analysis of basis factors by the eigenvalue analysis does not take concentration (intensity) information into account; therefore, the cross-validation (CV) technique, which accounts for both spectral and intensity information, is useful to ascertain the accuracy of the REV results.[18]

The root-mean-square prediction error of cross-validation (RMSECV) was also determined. RMSECV combines CV and the leave-one-out method and is given by[18]

$$RMSECV = \sqrt{\frac{\sum_{j=1}^{n} (\hat{c}_j - c_j)^2}{n}}, \quad (9)$$

where $\hat{c}_j$ and c_j are the predicted and actual concentrations, respectively, as determined by the reference method, and n is the number of samples used in the calibration model. The plot of RMESVE versus the number of principle components

normally has a break or a minimum at the true number of significant factors. In addition, factors that decrease RMSECV by <2% of the maximum RMSECV are usually rejected as error factors.[16] The use of both REV and RMSECV increases the accuracy of the PCA factor analysis.

Results and Discussion

SiO_2/water interface

Figure 2a shows the Raman spectra of the (a) SiO_2/air interface and (b) SiO_2/SAM/air interface. A broad band which is assigned to the SiO–H stretching of surface silanols with adsorbed water from the atmosphere is observed around 3550 cm^{-1} in Fig. 2a.[19,20] The Raman spectrum of the interface after attaching the SAM to the prism is shown in Fig. 2(b). The band around 2800 cm^{-1} to 3000 cm^{-1} is assigned to the CH stretching of the SAM, and the band around 3550 cm^{-1} might represent hydrogen-bonded silanols on the prism surface; these silanols are an unreactive moiety in the SAM coating. These results indicate the presence of some defects in the SAM layer.

Raman spectra of the SiO_2/water interface as a function of the angle of incidence are shown in Figs. 3a–e. The figures correspond to experimental incident angles of (a) 39°, (b) 46°, (c) 56°, (d) 64° and (e) 72°. The spectral shapes appear to be almost identical to each other and only the spectral intensity changes with the angle of incidence. These characteristics indicate that bulk water dominates the spectral changes due to the depth change of the evanescent field, while the contribution of boundary water is negligible.

PCA is unique in its ability to resolve the spectra of minute species from those of dominant species. This differentiation is readily achieved when the signal ratio of the

dominant species is within the range of 10^2 to 10^4; thus, the TIR Raman spectra for different angles of incidence (Fig. 3) were subjected to PCA to resolve the minute species.

As shown in Fig. 4a, the REV becomes significantly smaller at n = 4. This behaviour demonstrates the presence of three significant components in the data set. The eigenvalue of the 1st factor is much larger than those of the 2nd and 3rd factors, indicating that the 1st factor is the dominant component, while the 2nd and 3rd factors are minute components. RMSECV is also shown in Fig. 4b. In this case, after n = 3, the factor does not improve RMSECV by <2%, which also supports the conclusion that three significant components are present in the data set. Therefore, the REV and RMESVE results both indicate that there are one dominant and two minute species. The C_R values of the 1st, 2nd and 3rd PCA loadings are shown in Figs. S1a and S1b. As d_p decreases, the C_R of the first loading also decreases, whereas the C_R values of the second and third loadings increase. These results suggest that as d_p decreases, the contributions of the minute chemical species of the 2nd and 3rd loadings increase; in other words, these species are surface-specific. The 1st through 3rd PCA loadings are presented as spectra in Figs. 4c–e. Since the 1st PCA loading always yields the average spectrum, it is quite similar to the original spectrum corresponding to bulk water species. The 2nd PCA loading is, however, quite different from the 1st loading. In the 2nd PCA loading, there are two positive bands and one negative band. When mutually dependent chemical components are present in a sample, the resolved PCA loading should have negative bands due to the dependent component. One of the positive bands is a broad band at around at 3100 cm^{-1}, and the other is a relatively sharp band at 3550 cm^{-1}. The negative band is located at around 3400 cm^{-1}. The Raman bands of water are known to

be strongly affected by the hydrogen bonding network, and the wavenumbers of the Raman bands of water depend on the strength of the hydrogen bonding network.[21,22] Basically, lower-wavenumber Raman bands of water indicate a strong hydrogen bonding network, whereas higher-wavenumber bands correspond to a weak hydrogen bonding network. Hence, the band at 3100 cm^{-1} is assigned to water molecules with a strong hydrogen bonding network. On the other hand, the band at around 3400 cm^{-1} is assigned to partly hydrogen bounded water (liquid like water), which mainly constitutes bulky water. The 2nd loading spectrum has both the positive band at 3100 cm^{-1} and the negative band at around 3400 cm^{-1}, indicating that this spectrum has a relatively strong hydrogen bonding network compared to that of bulky water. In addition to these two bands, the 2nd loading spectrum has a sharp band at 3550 cm^{-1}, which is assigned to surface silanol groups H-bonded to molecular water.[20] Therefore, the 2nd PCA loading spectrum suggests that water molecules that are strongly hydrogen-bonded with surface silanol groups are present on the prism. Some previous studies supported this result and they indicated that the strongly hydrogen bonded water molecules has a well ordered structure at SiO_2/Water interface.[22-24]

The 3rd PCA loading spectrum has one positive band and one negative band: the positive band at 3600 cm^{-1} is assigned to the water molecules with a weak hydrogen bonding structure,[21,22] while the negative band at 3200 cm^{-1} is assigned to the water molecules with a strong hydrogen bonding structure. Therefore, the water molecules of the 3rd PCA loading spectrum have a hydrogen bonding network weaker than that of bulk water. A previous study indicated that asymmetrically ordered water with a weak hydrogen bonding network is present at the SiO_2/water interface;[23,24] thus, the 3rd PCA loading spectrum suggests that another spices of water molecules with an asymmetrical

structure is present on the prism surface. Thus, angle-resolved TIR Raman analysis revealed that there are two species of water molecules with different structures on the prism surface.

SAM/water interface

The Raman spectra of the SAM/water interface are shown in Figs. 5a–e as functions of the angle of incidence. The figures correspond to experimental incident angles of (a) 39°, (b) 46°, (c) 56°, (d) 64° and (e) 72°. The spectral shapes of the Raman bands of water are almost identical to each other; however, the sharp band at around 2850 cm^{-1} notably increases with increasing angle of incidence. The two sharp bands at 2850 cm^{-1} and 2890 cm^{-1} are assigned to the CH stretching band of ODS on the prism. These TIR Raman spectra at different angles of incidence (Fig. 5) were subjected to PCA. As shown in Fig. 6a, the REV becomes significantly smaller starting at n = 3. This REV behaviour demonstrates the presence of two significant components in the data set. The eigenvalue of the 1st factor is much larger than that of the 2nd factor, indicating that the 1st factor is the dominant component, while the 2nd is a minute component. The RMESVE is also shown in Fig. 6b. The RMESVE exhibits a break at n = 2, indicating that there are two principle components in the data set. Therefore, both the REV and RMESVE results indicate that this data set contains one main species and one minute species. The C_R values of the 1st, 2nd and 3rd PCA loadings are shown in Figs. S2a and S2b. As d_p decreases, the C_R of the 1st loading also decreases, whereas the C_R of the 2nd loading increase. This result suggests that as d_p decreases, the contribution of the minute chemical species of the 2nd loading to the measured spectrum increases, indicating that this minute species is a surface-specific component. The 1st and 2nd PCA loadings are

presented as spectra in Figs. 6c and 6d. Since the 1st PCA loading always yields the average spectrum, as it does for the SiO_2/water interface, it is quite similar to the original spectrum, which corresponds to that of bulk water. Notably, the 2nd PCA loading exhibits two sharp bands at 2850 cm^{-1} and 2890 cm^{-1}, which are assigned to the CH stretching band of ODS on the prism. A broad positive band is also observed around 3560 cm^{-1}, which is assigned to the surface silanol groups that are H-bonded to molecular water. There is also a broad negative band around 3200 cm^{-1}, which indicates that minute species of water molecules at the ODS/water interface have a hydrogen bonding network weaker than that of bulk water.

Under TIR conditions, the Raman intensity can be calculated by integrating the square of the evanescent field; therefore, if the intensity of a species is known, the thickness of the species can be estimated. Here, the eigenvalue is roughly proportional to the species intensity; thus, the thickness (h) of the species can be estimated from the eigenvalue according to

$$C_{\mathrm{R}} = \frac{\int_0^h E(x)^2 dx}{\int_0^\infty E(x)^2 dx}. \qquad (10)$$

In the case of an incident angle θ of 56°, which corresponds to an effective thickness (d_{eff}) of 40 nm, at the SiO_2/water interface, the C_R values of the 2nd and 3rd species are 0.028 and 0.0072, respectively. The calculated partially integrated values of C_R for the 2nd and 3rd species are 1.1 nm and 0.29 nm, respectively. In the same way, the average thickness of each species was estimated for each θ (or d_{eff}), and the thicknesses of the 2nd and 3rd species were estimated to be 1.1 nm ± 0.1 nm and 0.43 nm ± 0.1 nm,

respectively. The water molecule boundaries with thicknesses of 1.1 nm and 0.43 nm can be roughly estimated to consist of a few layers and a monolayer, respectively. Therefore, the water molecules with a strong hydrogen bonding network formed a few layers, while those with an asymmetrical structure composed almost one monolayer. A previous experimental study on the Si/water interface reported the similar result, although the studied system was not the same as that used in this study.[25] A previous theoretical study shows that the structure of absorbed water is affected by the orientation of the surface silanols.[26] It means that out of plane silanols form strong hydrogen bonds with water molecules at the interface, on the other hand in plane silanols form weak hydrogen bonds with the interfacial water. These results explain the existence of two species of absorbed water at the interface and support the result of this study.

In SAM/water interface, the thickness of water molecules at the SAM/water interface was also estimated. In the case of θ=56° (d_{eff} = 40 nm), the C_R of the 2nd species is 0.053, which corresponds to an average thickness of 2.2 nm. In the same way, the average thickness of the 2nd species was estimated for each θ (or d_{eff}); the average thickness was estimated to be 2.0 nm $\pm$ 0.1 nm, which is almost the same as the length of the main ODS chain (2.2 nm).[27] Thus, the thickness of the 2nd species is about the same as the size of ODS. This result suggests that the strongly hydrogen bonded water molecules were excluded by ODS, while the weakly hydrogen bonded water molecules remained. A previous study using vibrational sum frequency spectroscopy (VSFS) suggested that at the ODS/water interface at pH 7, there is no bonding between water and ODS and that the water structure on the SAM is mainly determined by the substrate charge. Therefore, weakly hydrogen bonded water molecules were not yielded from the

surface effect of the SAM.[28] Notably, in this study, defects in the SAM layer resulted in nanosized gaps between the SAM layers where small amounts of water molecules could enter (Fig. 7b). This prevents the hydrogen bonding network from completely developing, resulting in a weak hydrogen bonding network. A previous study determined that the water molecules at a mixed SAM interface formed a disordered structure with a Raman peak at around 3480 cm^{-1}.[29] Another previous study also showed that the water molecules in weakly coordinated environments, such as water molecules partially trapped within monolayer chains, have a peak near 3600 cm^{-1}.[24] Although these experiments were not performed on the system that was used in this study, both results indicate that the small amount of water in the nanoscale gaps between SAM layers is associated with an immature hydrogen bonding network. Therefore, these past results support those of the current study.[24]

In conclusion, our results indicate that two minute water species are present at the SiO_2/water interface: one is absorbed on the silanol groups of the prism and has a strong hydrogen bonding network with a thickness of a few layers; the other has an asymmetrical structure and a monolayer thickness. In contrast, at the SAM/water interface, a different kind of minute species with a weak hydrogen bonding network and a thickness that is almost the same as that of the SAM is present.

Thus, by using angle-resolved TIR Raman spectroscopy with PCA, the surface-specific minute species at the hydrophobic and hydrophilic interfaces were characterised, and their thicknesses were estimated. The combination of these techniques is expected to be powerful for water structure analyses at interfaces in aqueous systems and for the analyses of interactions between chemical species absorbed on surfaces. From a practical point of view, angle-resolved TIR Raman spectroscopy

will be advantageous in the analysis of interfacial water, which determines the hydrophobicity or hydrophilicity of an interface; therefore, this technique can be used to effectively evaluate the surface wettability of SAMs on a molecular level. Interfacial water also plays an important role in protein adsorption on polymer surfaces. Furthermore, this technique will be a powerful tool to investigate the biocompatibility or bioinertness of biomedical polymers.

Summary

Interfacial analyses of SiO_2/water and SAM/water systems were performed using angle-resolved TIR Raman spectroscopy with PCA analysis. The minute species at the interfaces were characterised, and their thicknesses were estimated. The combination of these techniques is expected to be powerful for the structural analysis of boundary phases in aqueous systems. This method will likely lead to progress in various surface and interfacial analyses, not only those related to the structure of water, but also those used to determine the interactions among absorbed species.

Supporting Information

The C_R values of each PCA loadings are shown as supporting information (Fig. S1 and S2).

References

1. X. D. Zhu, H. Suhr, and Y. R. Shen, *Phys. Rev. B*, **1987**,*35*, 3047 – 3050

2. Y. R. Shen, *Nature*, **1989**, *337*, 519 – 524

3. N. J. Everall, *Appl. Spectrosc.* **2009**, *63*, 245A-262A.

4. N. J. Everall, *Analyst* **2010**, *135*, 2512-2522.

5. S. G. Kazarian and K. L. A. Chan, *Appl. Spectrosc.* **2010**, *64*, 135A–151A.

6. B. L.Mojet, S. D. Ebbesen and L. Lefferts, *Chem. Soc. Rev.* **2010**, *39*, 4643–4655.

7. T. Ikeshoji, Y. Ono and T. Mizuno, *Appl. Opt*. **1973**, *12*, 2236–2237.

8. R. Iwamoto, M. Miya, K. Ohta and S. Mima, *J. Am. Chem. Soc*.**1980**, *102*, 1212–1213.

9. M. Ohsawa, K. Hashima and W. Suëtaka, *Appl. Surf. Sci*. **1984**, *20*, 109–120.

10. P. A. Greene and C. D. Bain, *Spectroscopy Europe* **2004** *16*, 8-15.

11. E. Tyrode, M. W. Rutland, C. D. Bain, *J. Am. Chem. Soc*. **2008**, *130*, 17434–17445.

12. D. A. Woods and C. D. Bain, *Analyst* **2012**, *137*, 35–48.

13. J. E. Bertie and K. H. Michaelian, *J. Chem. Phys*. **1998** *109*, 6764-6771.

14. M. D. Porter, T. B. Bright, D. L. Allara and T. Kuwana, *Anal. Chem.*, **1986,** *58*, 2461–2465.

15. D. A. Wood and C. D. Bain, *Soft Matter*, **2014**, *10*, 1071-1096.

16. E.R. Malinowski, *Factor Analysis in Chemistry* (2nd ed.); Wiley-Interscience: New York, 1991.

17. R. Parthasarathy, G. Thiagarajan, X. Yao, Y. Wang, P. Spencer, and Y. Wang, *J. Biomed. Opt.* **2008,** *13*, 014020-014020-9.

18. A. P. Lobo, B.S. Valles, N. F. Tascón, R.R. Madrera, *LWT Food Sci. & Tech.*, **2006**, *39*(9) 1026–1032.

19. C. P. Tripp and M. L. Hair, *Langmuir* **1992***, 8,* 1120-1126.

20. A. Anedda, C.M. Carbonaro, F. Clemente, L. Corda, R. Corpino, P. C. Ricci, *Mater. Sci. Eng. C* **2003**, *23* 1069–1072.

21. Q. Du, E. Freysz, Y. R. Shen, *Phy. Rev. Lett.* **1994**, *72*, 238-241.

22. Y. R. Shen and V. Ostroverkhov, *Chem. Rev.* **2006**, *106*, 1140-1154 1140.

23. Q. Du, E. Freysz, Y. R. Shen, Y. R. *Science* **1994**, *264*, 826.

24. A. J. Hopkins, C. L. McFearin and G. L. Richmond, *J. Phys. Chem. C* **2011**, *115*, 11192-11203.

25. D. B. Asay and S. H. Kim, *J. Phys. Chem. B* **2005,** *109,* 16760-16763.

26. M. Sulpizi, M. Gaigeot, M. Sprik, *J. Chem. Theory Comput*. **2012**, *8*, 1037–1047.

27. A. Hozumi, H. Sugimura, Y. Yokogawa, T. Kameyama, O. Takai, *Colloids Surf., A* **2001**, *182*, 257–261.

28. E. Tyrode and J. F. D. Liljeblad, *J. Phys. Chem. C* **2013**, *117*, 1780−1790.

29. Y. Tong, E. Tyrode, M. Osawa, N. Yoshida, T. Watanabe, A. Nakajima, and S. Ye, *Langmuir* **2011**, *27*, 5420–5426.

Figure captions

Figure 1. Schematic of TIR Raman measurement

Figure 2. Raman spectra of (a) SiO_2/air interface and (b) SAM/air interface

Figure 3. Raman spectra of SiO_2/water interface at different angles of incidence: (a) 39°, (b) 46°, (c) 56°, (d) 64° and (e) 72°

Figure 4. Plots of (a) reduced eigenvalue and (b) root-mean-square prediction error of cross-validation versus factor level, and (c) 1st, (d) 2nd and (e) 3rd PCA loading spectra of SiO_2/water interface

Figure 5. Raman spectra of SAM/water interface at different angles of incidence: (a) 39°, (b) 46°, (c) 56°, (d) 64° and (e) 72°

Figure 6. Plots of (a) reduced eigenvalue and (b) root-mean-square prediction error of cross-validation versus factor level, and (c) 1st, (d) 2nd and (e) 3rd PCA loading spectra of SAM/water interface

Figure 7. Schematic of (a) SiO_2/water interface and (b) SAM/water interface

Figure S1. Contribution ratios (C_R) of (a) first(●), (b) second (○) and third (◎) PCA loadings versus effective penetration depth (d_{eff})

Figure S2. Contribution ratios (C_R) of (a) first(●) and (b) second (○) PCA loadings versus effective penetration depth (d_{eff})

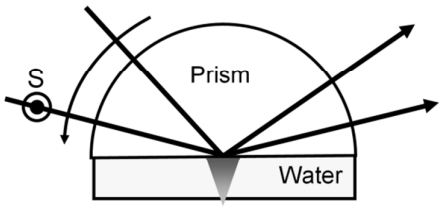

Figure 1. Schematic of TIR Raman measurement

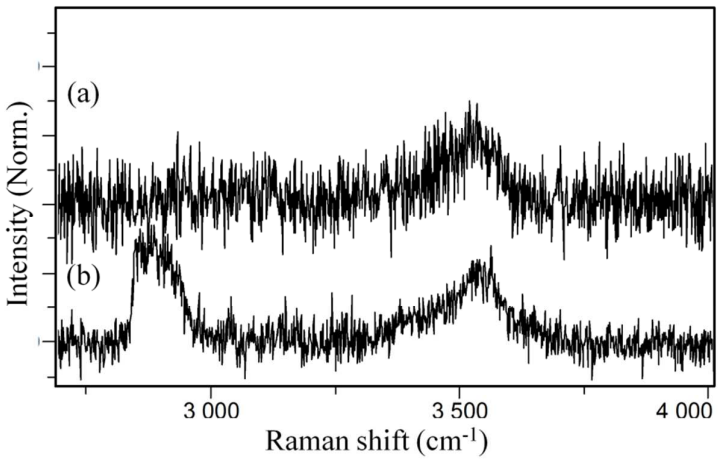

Figure 2. Raman spectra of (a) SiO_2/air interface and (b) SAM/air interface

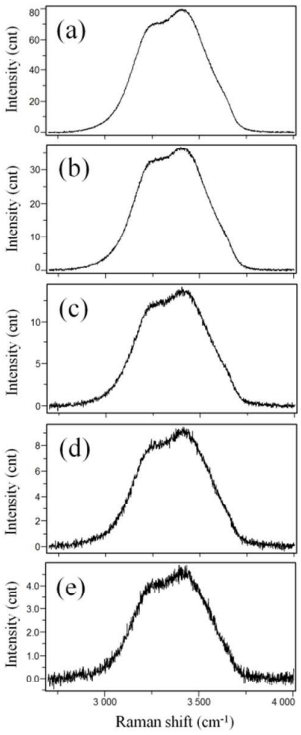

Figure 3. Raman spectra of SiO_2/water interface at different angles of incidence: (a) 39°, (b) 46°, (c) 56°, (d) 64° and (e) 72°

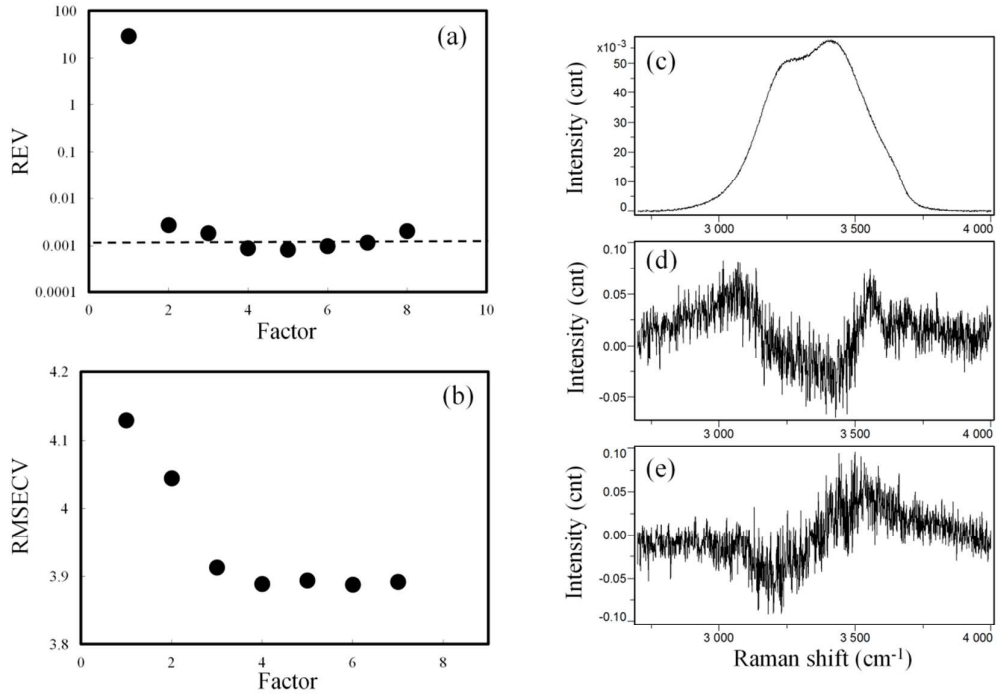

Figure 4. Plots of (a) reduced eigenvalue and (b) root-mean-square prediction error of cross-validation versus factor level, and (c) 1st, (d) 2nd and (e) 3rd PCA loading spectra of SiO_2/water interface

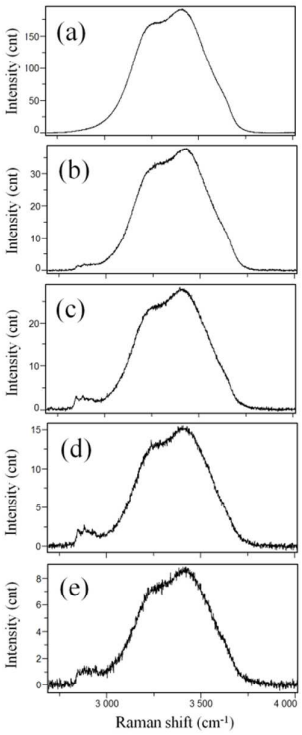

Figure 5. Raman spectra of SAM/water interface at different angles of incidence: (a) 39°, (b) 46°, (c) 56°, (d) 64° and (e) 72°

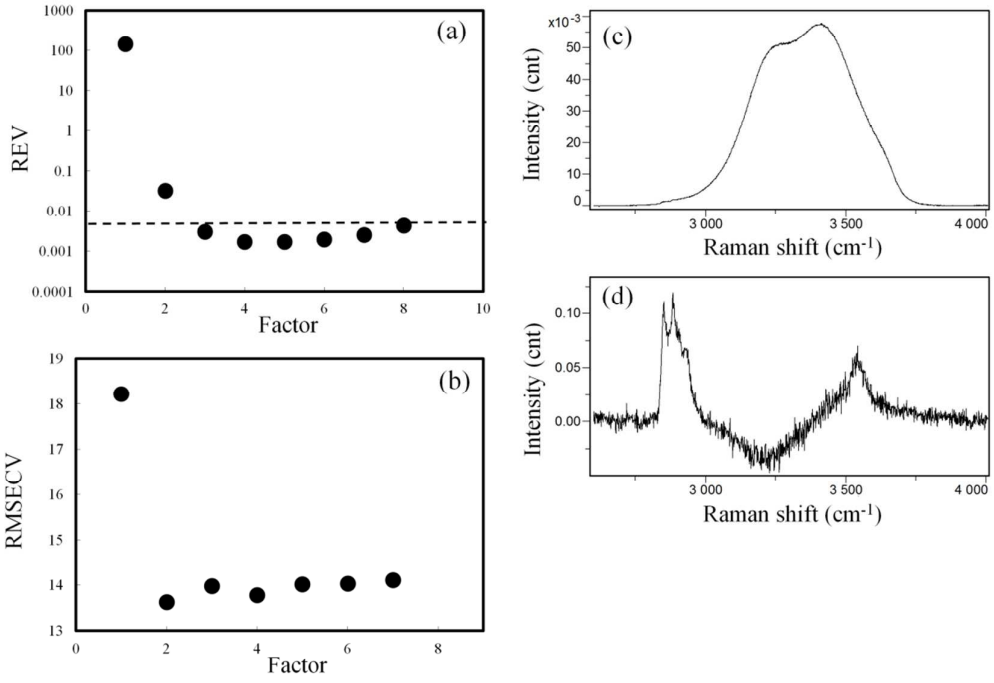

Figure 6. Plots of (a) reduced eigenvalue and (b) root-mean-square prediction error of cross-validation versus factor level, and (c) 1st, (d) 2nd and (e) 3rd PCA loading spectra of SAM/water interface

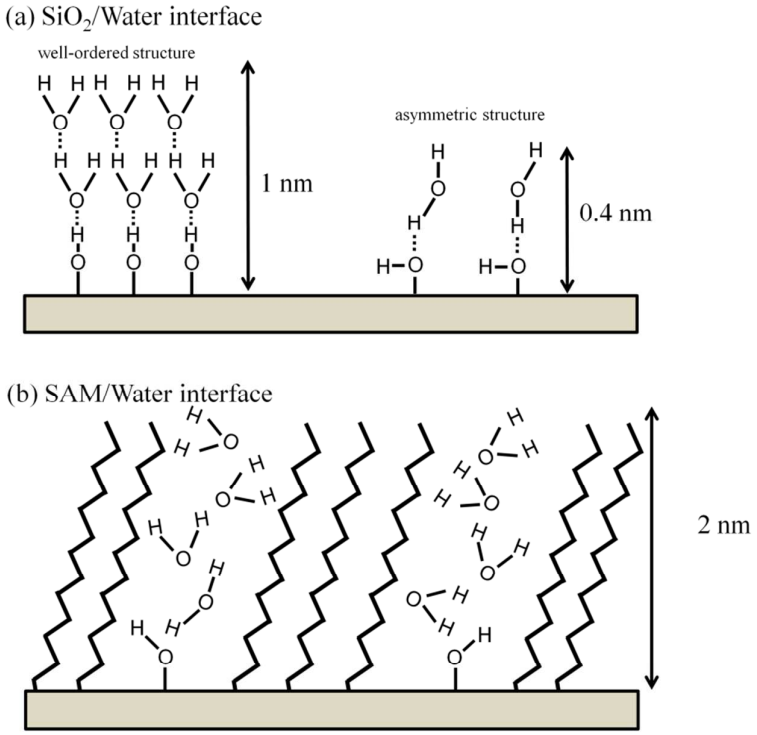

Figure 7. Schematic of (a) SiO_2/water interface and (b) SAM/water interface

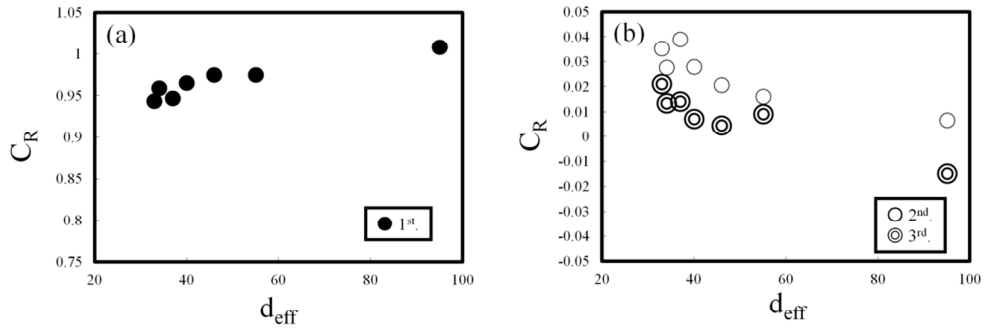

Figure S1. Contribution ratios (C_R) of (a) first(●), (b) second (○) and third (◎) PCA loadings versus effective penetration depth (d_{eff})

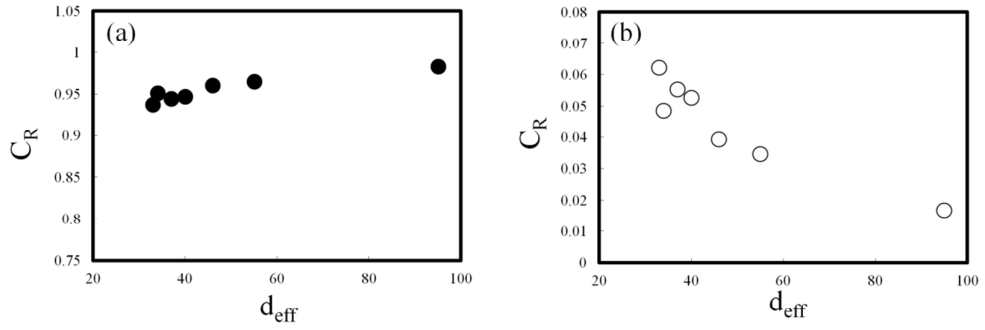

Figure S2. Contribution ratios (C_R) of (a) first(●) and (b) second (○) PCA loadings versus effective penetration depth (d_{eff})

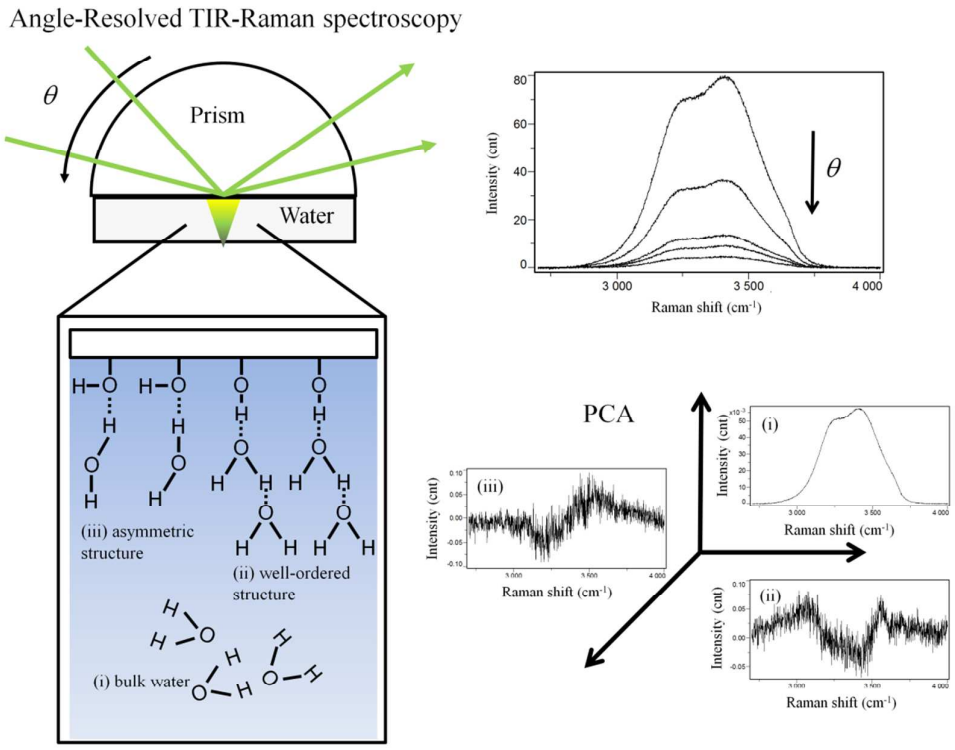

Graphical Abstract